JJC

Volume 18, Number 1, 2023
Pages 33–42

Jordan Journal of Chemistry
https://doi.org/10.47014/18.1.4

ARTICLE

Complexation of Selected Polycyclic Aromatic Hydrocarbons with Hexaprotonated Hexaazacyclophane Macrocycles

Danushka M. Kumarasinghe[a], Damith D. Lekamge[a], Suneth P. Rajapaksha[a], Isurika R. Fernando[a*]

Department of Chemistry, Faculty of Applied Sciences, University of Sri Jayewardenepura, Nugegoda 10250, Sri Lanka.

Received: 8th Jan. 2023; *Accepted:1st May 2023*

Abstract: This research focused on the host-guest complexation-driven detection of three selected polycyclic aromatic hydrocarbons (PAHs), naphthalene, anthracene and phenanthrene, in solution using two protonated hexaazacyclophane macrocycles ($\mathbf{1}^{6+}$), specifically $\mathbf{1a}^{6+}$ and $\mathbf{1b}^{6+}$. The geometry optimization of PAHs and $\mathbf{1}^{6+}$ performed using quantum chemical density functional theory calculations demonstrated their electronic compatibility to undergo host-guest complexation. The macrocycles $\mathbf{1a}^{6+}$ and $\mathbf{1b}^{6+}$, which possess different cavity geometries, were synthesized using [2+2] Schiff-base cyclization of diethylenetriamine separately with terephthalaldehyde and isophthalaldehyde, respectively, followed by reduction and protonation. After spectroscopic characterization of the macrocycles, the fluorescence spectroscopic determination of stoichiometry, binding constant and quenching constant between $\mathbf{1a}^{6+}$/$\mathbf{1b}^{6+}$ and PAH was performed using the Job's plot method, Benesi-Hildebrand method and Stern-Volmer plot, respectively. The stoichiometry of each combination of $\mathbf{1}^{6+}$ with PAH exhibits a 1:1 complexation. Among the PAHs studied, phenanthrene demonstrated the highest binding and quenching constants with both $\mathbf{1}^{6+}$, while anthracene and naphthalene showed the lowest binding and quenching constants, respectively, with both $\mathbf{1}^{6+}$. The cavity geometry of $\mathbf{1}^{6+}$ and the shape and number of fused rings of PAHs contributed to the binding constant.

Keywords: Supramolecular chemistry, Host-guest chemistry, Job's plot, Benesi-Hildebrand method, Stern-Volmer plot.

Introduction

Polycyclic aromatic hydrocarbons (PAHs) are a class of organic compounds of carbon and hydrogen, forming two or more fused aromatic rings[1–5]. Natural phenomena, including volcanic eruptions and forest fires, and anthropogenic activities, including incomplete combustion of fossil fuels, are responsible for more than 100 ubiquitous PAHs in the environment[1–5]. The chemical and physical properties of PAHs, such as hydrophobicity, low solubility in water, high solubility in lipids and slow degradation, facilitate the accumulation of PAHs in the environment and biological systems while causing harmful effects on flora and fauna[1–8].

Therefore, a wide range of chemical, physical and biological strategies have been developed to mobilize, immobilize or degrade the toxic and carcinogenic PAHs accumulated in the environment[2,4,9–16]. Among them, the conversion of PAHs to less toxic or non-toxic substances with the aid of biological species or light has been used in bio/microbial and photochemical degradation, respectively[2,4,9–13]. In the wet and dry deposition methods, PAHs absorbing atmospheric particles settle on Earth in the presence or absence of precipitation, respectively[14].

Furthermore, a supramolecular approach of secondary interactions-driven host-guest complex formation between the 'guest' molecule

[*]**Corresponding Author:** Isurika R. Fernando **Email**: isurika.fernando@sjp.ac.lk

PAH and a compatible macrocyclic 'host' molecule has been used to extract PAHs from various sources[17,18]. The host-guest complexation between the hydrophobic inner cavity of toroidal-shaped cyclodextrin (CD) or derivatized CD and electron-rich hydrophobic PAHs through the formation of intermolecular hydrophobic interactions and/or hydrogen bonding, the release of high-energy water molecules from the CD cavity, or combination of these interactions and phenomena have been utilized to remove PAHs from the atmosphere, air and soil[17,19]. The π-π stacking and hydrogen bonding-driven encapsulation of PAHs in the cavity of calixarenes has been used to remove PAHs from the environment[18,20]. The π-π stacking, hydrogen bonding, and hydrophobic interactions-directed self-assembly of electron-deficient diazapyrenium-based palladium(II)- and platinum(II)-containing metallocycles and PAHs have been investigated with the intention of detecting and removing PAHs[21]. A neutral fluorenone-based triazolophane macrocycle demonstrated sensing abilities for PAHs via co-facial interactions between fluorenone and biphenyl units of the macrocycle and a couple of selected PAHs[22]. Moreover, another neutral macrocycle of perylene bisimide cyclophane exhibited a high binding affinity towards planar PAHs, anthracene, perylene and pyrene[23]. The Stoddart group investigated the donor-acceptor interactions-driven host-guest complex formation between PAHs and electron-deficient, tetra-cationic cyclophanes, namely, ExBox and Ex2Box, as well as the hexa-cationic extended pyridinium-based cage-like molecule, specifically, ExCage which have been used as a potential method to scavenge PAHs from crude oil[24–26].

Although PAHs demonstrated a stronger binding affinity towards charged cyclophanes than to neutral macrocycles, such as CDs and calixarenes, the synthesis of certain cyclophanes is associated with several limitations, including the necessity of comparatively expensive starting materials, sophisticated reaction conditions, trained labor with knowledge and expertise on organic synthesis, a relatively long reaction time and low yield of the product[17–20,24–26]. To overcome these limitations, cost-effective, comparatively synthetically feasible protonated hexaazacyclophane macrocycles ($\mathbf{1}^{6+}$), specifically $\mathbf{1a}^{6+}$ and $\mathbf{1b}^{6+}$, that possess different cavity geometries (Figure 1) have been used as 'host' molecules in this study. This research project focused on the geometry optimization of $\mathbf{1}^{6+}$ and PAHs using quantum chemical density functional theory (DFT) calculations followed by the study on host-guest complexation, stoichiometries, binding and quenching behaviors of the resulting complexes of $\mathbf{1}^{6+}$ and PAHs in solution. This study is to date, to the best of our knowledge, the first systematic research on host-guest chemistry and quenching behavior of electron-deficient protonated hexaazacyclophane macrocycles, $\mathbf{1a}^{6+}$ and $\mathbf{1b}^{6+}$, with three selected electron-rich PAHs. Subsequently, the findings of this reporting study provide a fundamental understanding and a proper direction for the complexation-driven separation of PAHs from PAH-contaminated water.

Materials and Methods

All chemicals and solvents were of analytical grade and used as received from chemical suppliers without further purification unless otherwise mentioned. Analytical balance (Precisa Instruments Ltd, max: 200 g, min: 0.0001 g), rotary evaporator (Heidolph Laborota 4000) and stirrer hotplate (Labtech LMS-1003) were used in this work. The UV-Visible spectra and fluorescence spectra were recorded on the UV-visible spectrophotometer Thermo Scientific GENESYS 10S and the fluorescence spectrometer Thermo Scientific LUMINA, respectively, using a quartz cuvette with 1.0 cm path length. The UV-Visible and fluorescence spectra were processed with UV WIN and WAVE SCAN software, respectively. The Fourier transform infrared (FTIR) spectra were recorded on the FTIR spectrometer Thermo Scientific NICOLET iS10, and the spectral data were processed with OMNIC software. The proton nuclear magnetic resonance (^{1}H NMR) spectra were recorded in $CDCl_3$ using NMR spectrometer (Bruker Ascend 400 MHz) at 298 K. ^{1}H NMR data were analyzed using SpinWorks software.

Density Functional Theory (DFT) Calculations

Quantum chemical DFT calculations were performed using ORCA version 4.0.1.2. The geometry optimizations of $\mathbf{1}^{6+}$ and PAHs were carried out using the Becke-3-Lee-Yang-Parr (B3LYP) function along with the def2-SVP basis set. The solvent was treated with a conductor-like polarizable continuum model.

Synthesis and Characterization of Protonated Hexaazacyclophane Macrocycles

Two protonated hexaazacyclophane macrocycles, $\mathbf{1a}^{6+}$ and $\mathbf{1b}^{6+}$, were synthesized (Figure 1) using modified literature procedures that involve the [2+2] Schiff-base condensation of terminal diamine and dialdehyde followed by reduction and protonation[27–31]. Diethylenetriamine (DETA) was used as the terminal diamine for the synthesis of both $\mathbf{1}^{6+}$, while terephthalaldehyde (TPA) and isophthalaldehyde (IPA) were used as dialdehyde for $\mathbf{1a}^{6+}$ and $\mathbf{1b}^{6+}$, respectively. The synthesized compounds were characterized using UV-visible, FTIR, and ^{1}H NMR spectroscopy.

3,6,9,16,19,22-Hexaazatricyclo-[22.2.2.2^{11,14}] triaconta-1(27),2,9,11(30),12,14(29),15,22, 24(28),25-decaene ***2a***

Yellow powdery precipitate (55 ± 3.51%). m.p. 155–157 ºC; R_f = 0.48 (SiO_2, MeOH-CH_2Cl_2, 1:4); UV-Vis (CH_2Cl_2): λ_{max}, 270 nm; FTIR (ATR): ν (cm^{-1}), 3304 (–N–H), 2921 (–C–H), 1644 (–CH=N–), 824 (*para*-substituted phenylene ring). ^{1}H NMR ($CDCl_3$, 400 MHz, 298 K): δ (ppm), 8.297 (s, 4H, –CH=N–), 7.537 (s, 8H, Ar), 3.797 (t, 8H, *J* = 4.6 Hz, –CH_2–N=), 3.005 (t, 8H, *J* = 5.2 Hz, –CH_2–NH–).

3,6,9,17,20,23-Hexaazatricyclo-[23.3.1.1^{11,15}] triaconta-1(29),2,9,11(30),12,14,16,23,25,27-decaene ***2b***

White powdery precipitate (33.6 ± 1.65%). m.p. 152–154 ºC; R_f = 0.49 (SiO_2, MeOH-CH_2Cl_2, 1:4); UV-Vis (CH_2Cl_2): λ_{max}, 244 nm; FTIR (ATR): ν (cm^{-1}), 3315 (–N–H), 2789 (–C–H), 1647 (–CH=N–), 790 (*meta*-substituted phenylene ring); ^{1}H NMR ($CDCl_3$, 400 MHz, 298 K): δ (ppm), 8.098 (s, 4H, –CH=N–), 7.517 (d, 2H, *J* = 7.6 Hz, Ar), 7.365 (m, 6H, Ar), 3.754 (t, 8H, *J* = 7.4 Hz, –CH_2–N=), 3.570 (t, 8H, *J* = 11.4 Hz, –CH_2–NH–).

3,6,9,16,19,22-Hexaazatricyclo-[22.2.2.2^{11,14}] triaconta-1(27),11(30),12,14(29),24(28),25-hexaene ***3a***

Pale yellow precipitate (96.0 ± 2.25%). R_f = 0.34 (SiO_2, MeOH-CH_2Cl_2, 1:5); UV-Vis (CH_2Cl_2): λ_{max}, 242 nm; FTIR (ATR): ν (cm^{-1}), 3333 (–N–H), 2798 (–C–H), 1445 (–C–H), 1110 (–C–N), 810 (*para*-substituted phenylene ring); ^{1}H NMR ($CDCl_3$, 400 MHz, 298 K): δ (ppm), 7.181 (s, 8H, Ar), 3.692 (s, 8H, Ar–CH_2–), 2.742 (m, 8H, –NH–CH_2–), 2.698 (m, 8H, –CH_2–NH).

3,6,9,17,20,23-Hexaazatricyclo[23.3.1.1^{11,15}] triaconta-1(29),11(30),12.14,25,27-hexaene **3b**

Colorless viscous liquid (86.4 ± 1.04%). R_f = 0.45 (SiO_2, MeOH-CH_2Cl_2, 1:5); UV-Vis (CH_2Cl_2): λ_{max}, 242 nm; FTIR (ATR): ν (cm^{-1}), 3150 (–N–H), 2789 (–C–H), 1456 (–C–H), 1061 (–C–N), 690 (*meta*-substituted phenylene ring); ^{1}H NMR ($CDCl_3$, 400 MHz, 298 K): δ (ppm), 7.079 (d, 2H, *J* = 12.8 Hz, Ar), 7.132 (m, 4H, Ar), 7.281 (s, 2H, Ar), 3.681 (s, 8H, Ar–CH_2–), 2.634 (m, 16H, –CH_2–NH–).

General Procedure for $\boldsymbol{1^{6+}}$

Perchloric acid ($HClO_4$) (0.7 mL, 8.1 mmol, 1.76 g cm^{-3}) was added to a stirring solution of **3** (0.5012 g, 1.2 mmol) in ethanol (40 mL). The resulting precipitate was recrystallized using diethyl ether and CH_3CN to obtain $\mathbf{1{\cdot}6ClO_4}$.

3,6,9,16,19,22-Hexaazatricyclo[22.2.2.2^{11,14}] triaconta-1(27),11(30),12,14(29),24(28),25-hexaene hexakis(perchlorate) $\mathbf{1a{\cdot}6ClO_4}$

Light yellow precipitate (95.4 ± 3.12%). R_f = 0.30 (SiO_2, MeOH-CH_2Cl_2, 1:1); UV-Vis (CH_3CN): λ_{max}, 216 nm; FTIR (ATR): ν (cm^{-1}), 3420 (–N–H), 2775 (–C–H), 1567 (–C–H), 815 (*para*-substituted phenylene ring); ^{1}H NMR ($CDCl_3$, 400 MHz, 298 K): δ (ppm), 10.002 (s, 12H, –NH_2^+–), 7.242 (s, 8H, Ar), 6.811 (s, 8H, Ar–CH_2–), 5.753 (t, 8H, *J* = 6.2 Hz, –NH_2^+–CH_2–), 5.665 (t, 8H, *J* = 6.2 Hz, –CH_2–NH_2^+–).

3,6,9,17,20,23-Hexaazatricyclo[23.3.1.1^{11,15}] triaconta-1(29),11(30),12,14,25,27-hexaene hexakis (perchlorate) $\mathbf{1b{\cdot}6ClO_4}$

White precipitate (88 ± 1.04%). R_f = 0.44 (SiO_2, MeOH-CH_2Cl_2, 1:1); UV-Vis (CH_3CN): λ_{max}, 192 and 206 nm; FTIR (ATR): ν (cm^{-1}), 3151 (–N–H), 1051 (–C–N), 1581 (–C–H), 770 (*meta*-substituted phenylene ring); ^{1}H NMR ($CDCl_3$, 400 MHz, 298 K): δ (ppm), 10.002 (s, 12H, –NH_2^+–), 7.526 (s, 6H, Ar), 7.492 (s, 2H, Ar), 4.702 (s, 8H, Ar–CH_2–), 4.307 (m, 16H, –CH_2–NH_2^+–).

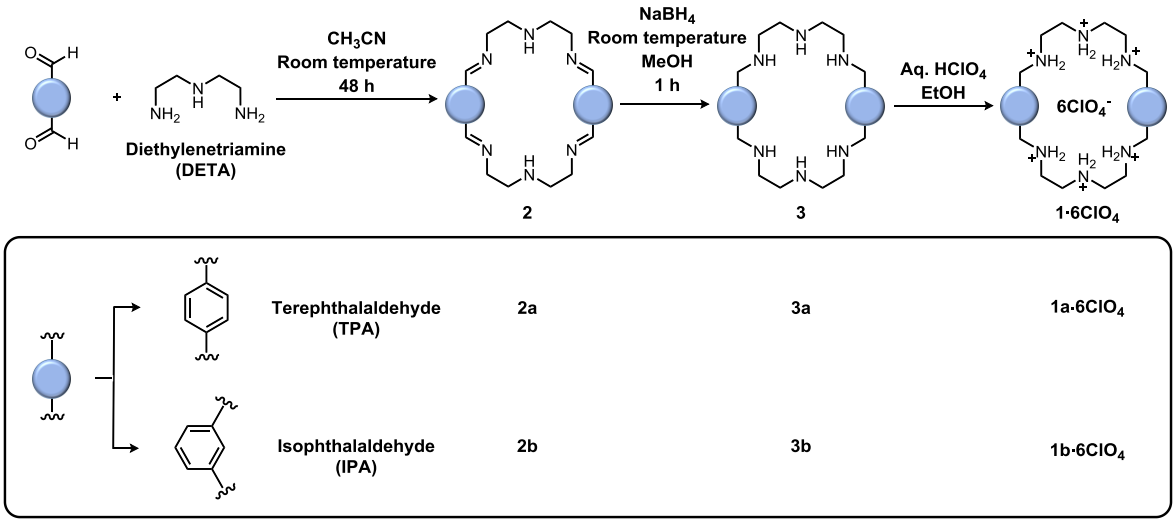

Figure 1. Synthesis scheme of $\mathbf{1}^{6+}$.

Spectroscopic Investigation of the Complexation of $\mathbf{1}^{6+}$ with PAHs

Acetonitrile was used as a solvent in the UV-vis and fluorometric study of the complexation of $\mathbf{1}^{6+}$ with PAHs. The UV-visible spectra were recorded in the wavelength range of 190–500 nm. The fluorescence emission spectra were recorded at excitation wavelengths of 270, 360, 305, 216 and 206 nm for naphthalene, anthracene, phenanthrene, $\mathbf{1a}^{6+}$ and $\mathbf{1b}^{6+}$, respectively. The fluorescence spectra of solutions of $\mathbf{1}^{6+}$ and PAHs were recorded at the excitation wavelength of the corresponding PAH.

For the qualitative study on the complexation of $\mathbf{1}^{6+}$ and PAHs, solutions of 0.0005 M of $\mathbf{1}^{6+}$, PAHs and a 1:1 mixture of $\mathbf{1}^{6+}$ and PAHs were prepared using 0.001 M standard stock solutions of $\mathbf{1}^{6+}$ and PAHs. The UV-visible spectra and the fluorescence spectra of each solution were recorded.

The stoichiometry between each combination of $\mathbf{1}^{6+}$ and PAH was determined using the Job's plot method and the dilution method[32,33]. For the Job's plot method, a series of solutions was prepared by mixing appropriate volumes of standard stock solutions of 0.001 M $\mathbf{1}^{6+}$ with 0.001 M PAH to obtain $\mathbf{1}^{6+}$:PAH molar ratios of 1:9, 2:8, 3:7, 4:6, 5:5, 6:4, 7:3, 8:2, and 9:1 in a total volume of 3.00 mL. Two other similar solution series were prepared where in one of them, the needed volume of standard stock solution of $\mathbf{1}^{6+}$ was replaced with acetonitrile, and in the other, the needed volume of standard stock solution of PAHs was replaced with acetonitrile. The fluorescence spectra of each prepared solution were recorded. The Job's plots for the complexation of $\mathbf{1a}^{6+}$ or $\mathbf{1b}^{6+}$ with each PAH were developed using the fluorescence intensity differences between each PAH solution and the corresponding mixture of the series of solutions at the relevant excitation wavelength.

In the dilution method, a volume of 2.00 mL of 0.0025 M PAH was titrated with 0.01 M $\mathbf{1}^{6+}$ solution in acetonitrile in a quartz cell. A volume of 0.10 mL of 0.01 M $\mathbf{1}^{6+}$ solution was added at a time until the added total volume of $\mathbf{1}^{6+}$ became 1.00 mL. The addition of 0.01 M $\mathbf{1}^{6+}$ solution continued by adding 0.50 mL at a time until the added total volume of 0.01 M $\mathbf{1}^{6+}$ became 2.50 mL. After each addition, the fluorescence spectrum of the resulting mixture was recorded. The graphs of fluorescence intensity versus concentration of $\mathbf{1}^{6+}$ were plotted for each combination of $\mathbf{1}^{6+}$ and PAH.

For the determination of the binding constants between $\mathbf{1}^{6+}$ and PAHs, the fluorescence spectroscopic data obtained from the titration explained under the 'dilution method' above was treated with the Benesi-Hildebrand equation (eq. 1) to construct the Benesi-Hildebrand plot [33–34].

$$\frac{1}{(\mathbf{I}-\mathbf{I_{min}})} = \frac{1}{[(\mathbf{I_{max}}-\mathbf{I_{min}})\mathbf{K_a}[\mathbf{C}]]} + \frac{1}{(\mathbf{I_{max}}-\mathbf{I_{min}})} \qquad (1)$$

where I_{min} is the emission intensity of PAH in the absence of $\mathbf{1}^{6+}$, I is the emission intensity in the presence of $\mathbf{1}^{6+}$, I_{max} is the emission intensity at a maximum concentration of $\mathbf{1}^{6+}$, K_a is the binding constant, and [C] is the concentration of $\mathbf{1}^{6+}$. K_a

can be calculated using the Benesi-Hildebrand plot, a plot of $1/(I - I_{min})$ against 1/[C].

To determine the quenching constant between $\mathbf{1}^{6+}$ and PAHs, the fluorescence data obtained from the fluorimetric titration explained under the 'dilution method' above was treated with the Stern-Volmer equation (eq. 2) to construct the Stern-Volmer plots [35,36].

$$\frac{I_{min}}{I} = 1 + K_{sv}[Q] \qquad (2)$$

where, I_{min} is the PAH emission intensity in the absence of $\mathbf{1}^{6+}$, I is the emission intensity in the presence of $\mathbf{1}^{6+}$, K_{sv} is the Stern–Volmer quenching constant and [Q] is the concentration of quencher, $\mathbf{1}^{6+}$ in this experiment. K_{sv} of each combination of $\mathbf{1}^{6+}$ and PAH was obtained from the corresponding Stern-Volmer plot, a plot of I_{min}/I against [Q].

Results and Discussion

DFT Calculations

In order to determine the tendency to undergo host-guest complexation between $\mathbf{1}^{6+}$ and PAHs, the compatibility of the geometrical and electronic properties of $\mathbf{1}^{6+}$ and PAHs was investigated using DFT calculations (Figure 2). The geometry optimization of $\mathbf{1a}^{6+}$ demonstrates a well-defined cavity with 10.03 Å distance between the *p*-substituted phenylene rings and 6.44 Å N-to-N distance between the central N atom of the two $–NH_2(CH_2)_2NH_2(CH_2)_2NH_2–$ chains opposite to each other in $\mathbf{1a}^{6+}$ (Figure 2a(i)). Similarly, the most stable 'chair-like' *trans* conformation of $\mathbf{1b}^{6+}$ obtained from the geometry optimization exhibits C-to-C distances of 10.49 to 10.57 Å for the two oppositely directed *m*-substituted phenylene rings and 5.42 Å and 6.53 Å N-to-N distances between the two terminal N atoms of the two opposite $–NH_2(CH_2)_2NH_2(CH_2)_2NH_2–$ groups in $\mathbf{1b}^{6+}$ (Figure 2a(ii)). The geometry-optimized structure of naphthalene exhibits dimensions of 6.78 Å and 5.01 Å for the highest length and width, respectively. Furthermore, the longest length and width of geometry-optimized structures of anthracene and phenanthrene are 9.24 Å, 5.01 Å and 9.32 Å, 5.59 Å, respectively. The electron density mapping of $\mathbf{1a}^{6+}$ and $\mathbf{1b}^{6+}$ demonstrates an electron-deficient cavity while that of PAHs exhibits the electron-rich core (Figure 2b). Therefore, the dimensions and electronic properties of $\mathbf{1}^{6+}$ make them compatible to undergo complexation with PAHs.

Synthesis and Characterization of Macrocycles

[2+2] Imine metathesis between terminal diamine groups of DETA with the dialdehyde TPA or IPA yields the hexaaza Schiff-base macrocycles **2a** or **2b**, respectively. Reduction with the reducing agent, sodium borohydride, yields the corresponding hexaazacyclophanes **3a** and **3b**. Protonation of **3** with mineral acids yields the protonated hexa-cationic hexaaza-cyclophanes $\mathbf{1a}^{6+}$ and $\mathbf{1b}^{6+}$ (Figure 1). The protonation of **3** with a series of mineral acids, HCl, HBr, HNO_3, H_2SO_4 and $HClO_4$, yields the aqueous-soluble **1**·6Cl, **1**·6Br, **1**·$6NO_3$, **1**·$3SO_4$ and **1**·$6ClO_4$, respectively. Among these salts of $\mathbf{1}^{6+}$, **1**·6Cl and **1**·6Br are insoluble in common organic solvents, while **1**·$6NO_3$ and **1**·$3SO_4$ are soluble in ethanol and methanol. **1**·$6ClO_4$ is soluble in acetonitrile and acetone, as well as in methanol and ethanol. These observations show that the counter ion of $\mathbf{1}^{6+}$ plays a significant role in the solubility of $\mathbf{1}^{6+}$ in different solvents.

Complexation between $\mathbf{1}^{6+}$ and PAHs

The UV-visible spectrum of $\mathbf{1}^{6+}$ in acetonitrile exhibits a characteristic intense band around 195 nm, while those of PAHs in acetonitrile show strong absorption band in the range 220–260 nm. These absorbance bands are attributed to the aromatic π–π* electronic transitions in these compounds (Figure 3a)[5]. The UV-visible spectra of the 1:1 molar mixture of 'host' and 'guest' in acetonitrile are equivalent to the summation of individual UV-visible spectra of the corresponding PAH and $\mathbf{1}^{6+}$ (Figure 3a). This result demonstrates the absence of significant complexation-induced absorbance changes.

The fluorescence spectra of $\mathbf{1a}^{6+}$ and $\mathbf{1b}^{6+}$ in acetonitrile indicate that both macrocycles are fluorescence-inactive, while those of naphthalene, anthracene and phenanthrene demonstrate characteristic intense bands corresponding to the transition from the singlet first excited state to the singlet ground state of conjugated aromatic rings (Figure 3b)[22,23]. The fluorescence spectra of the 1:1 molar mixture of $\mathbf{1}^{6+}$ and PAH in acetonitrile show a significant reduction in the fluorescence intensity of PAHs, attributed to the fluorescence quenching caused by the complexation of $\mathbf{1}^{6+}$ with PAH.

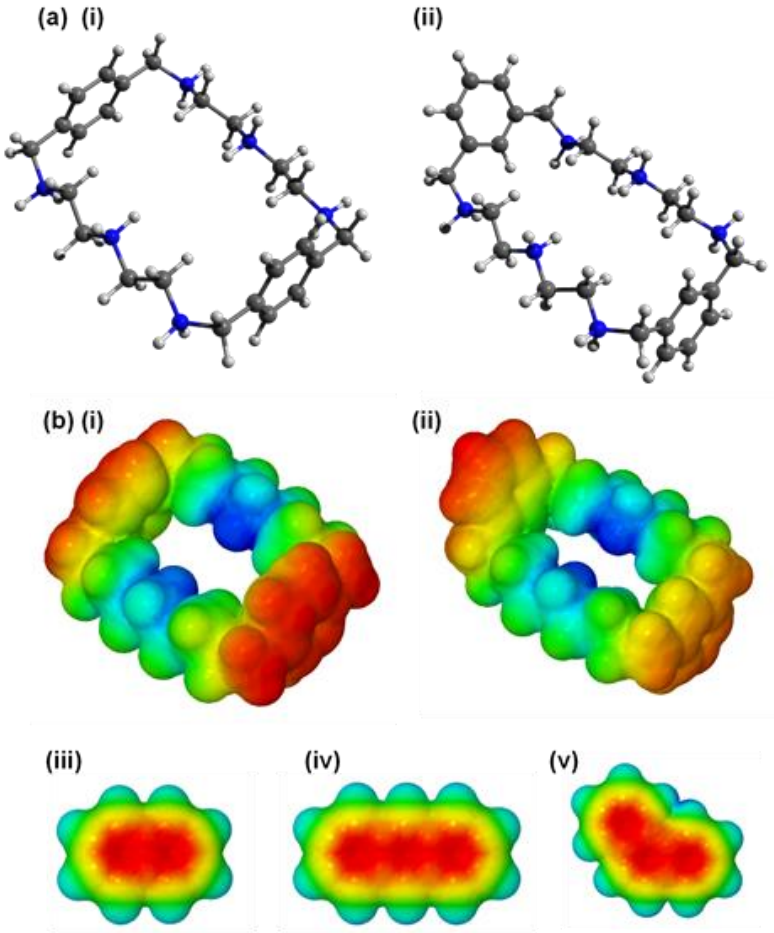

Figure 2. (a) Geometry optimized (B3LYP/def2-SVP) structures of (i) $1a^{6+}$ and (ii) $1b^{6+}$; (b) electron density mapping of 1^{6+}, (i) $1a^{6+}$, (ii) $1b^{6+}$, and PAH, (iii) naphthalene, (iv) anthracene, and (v) phenanthrene. Blue and red regions in each electron density map represent intramolecular electron-deficient and electron-rich regions, respectively. The colors of molecular electron density maps are not comparable with each other.

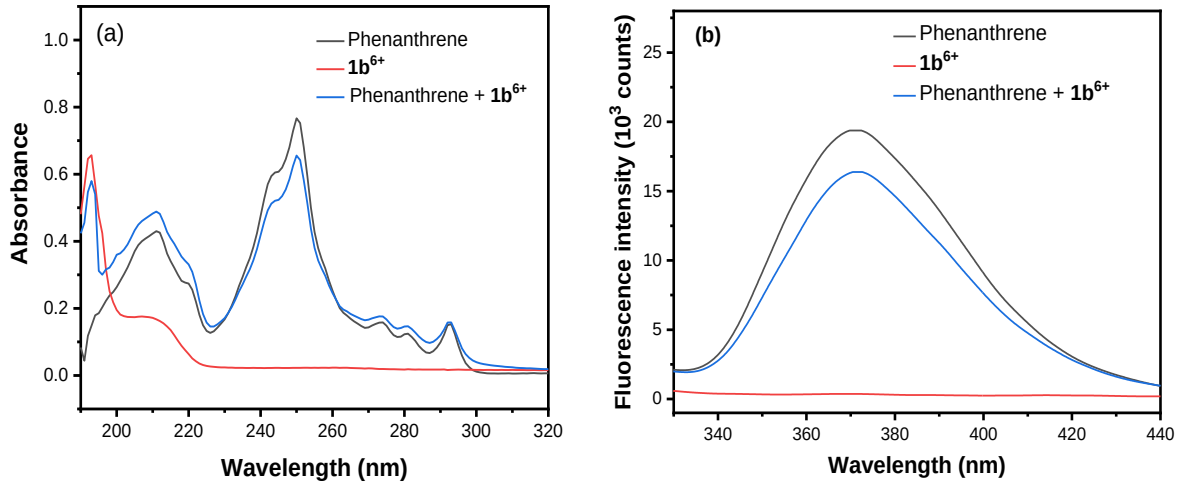

Figure 3. (a) UV-Visible and (b) fluorescence spectra of 0.0005 M phenanthrene, $1b^{6+}$ and a 1:1 mixture of $1b^{6+}$ and phenanthrene at 30 °C. Fluorescence emission spectra of phenanthrene, $1b^{6+}$ and a 1:1 mixture of $1b^{6+}$ and phenanthrene were recorded at excitation wavelengths of 305, 206 and 305 nm, respectively.

The Job's plots for each combination of $\mathbf{1}^{6+}$ and PAHs were constructed to deduce the complex stoichiometry in all $\mathbf{1}^{6+}$-PAH combinations. Figure 4a represents the Job's plot for the $\mathbf{1b}^{6+}$-phenanthrene complex. All formed complexes exhibit 1:1 stoichiometry between $\mathbf{1}^{6+}$ and PAH (Table 1). The plots of fluorescence intensity of the mixture versus the molar fraction of the macrocycle (Figure 4b for $\mathbf{1b}^{6+}$-phenanthrene complex as an example) demonstrates further the 1:1 binding stoichiometry confirming the results of the Job's plot method.

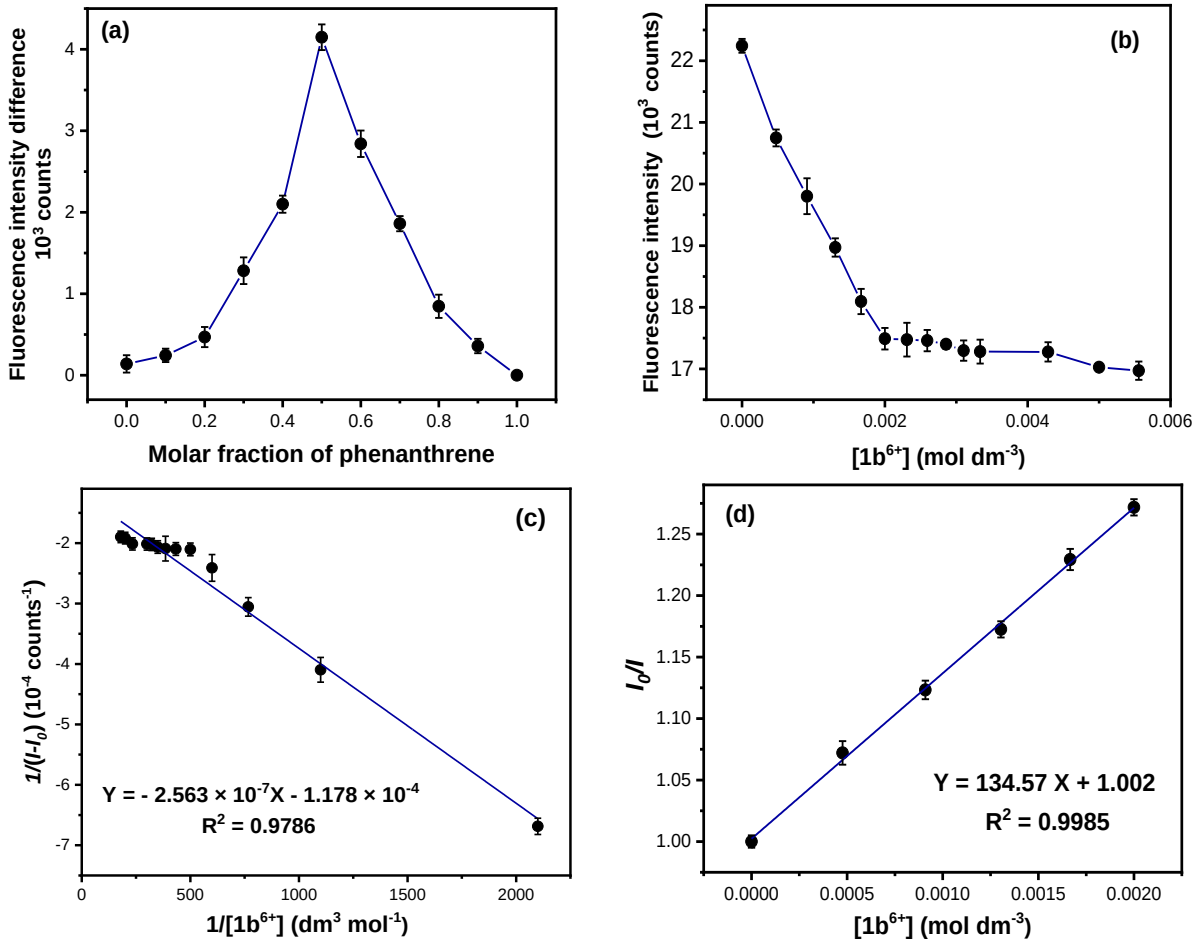

Figure 4 (a) Job's plot, (b) Fluorescence intensity vs. $\mathbf{1b}^{6+}$ concentration plot, (c) Benesi-Hildebrand plot and (d) Stern-Volmer plot of $\mathbf{1b}^{6+}$ and phenanthrene complexation study.

The Benesi-Hildebrand plots (Figure 4c for $\mathbf{1}^{6+}$-PAH as an example) give the values of the binding constants K_a which are listed in Table 1 for all six combinations between $\mathbf{1}^{6+}$ and PAHs in acetonitrile at 30°C. Among the three PAHs studied in this project, the 14-π electrons containing phenanthrene shows the highest K_a values of 495.84 ± 2.65 dm^3 mol^{-1} and 459.61 ± 1.96 dm^3 mol^{-1} for the complexation with $\mathbf{1a}^{6+}$ and $\mathbf{1b}^{6+}$, respectively (Table 1). On the contrary, the complexation of anthracene with $\mathbf{1a}^{6+}$ and $\mathbf{1b}^{6+}$ exhibits the lowest K_a values of 410.42 ± 0.75 dm^3 mol^{-1} and 340.91 ± 0.66 dm^3 mol^{-1}, respectively. Among the three PAHs studied in this project, phenanthrene demonstrates the highest aromaticity and stability compared to the 10-π electrons containing naphthalene and the linear acene of phenanthrene, anthracene[37]. The relatively high delocalization of the π electron cloud of phenanthrene leads to the formation of a relatively strong π–π stacking with $\mathbf{1a}^{6+}$ and $\mathbf{1b}^{6+}$. Therefore, phenanthrene tends to form complexes with electron-deficient $\mathbf{1}^{6+}$ than anthracene and naphthalene[37,38]. Among the protonated hexaazacyclophanes used in this study, $\mathbf{1a}^{6+}$ demonstrates higher K_a than $\mathbf{1b}^{6+}$ with naphthalene, anthracene and phenanthrene. Although $\mathbf{1a}^{6+}$ and $\mathbf{1b}^{6+}$ possess the same 6+

charge this observation is attributed to the differences of the cavity geometry of macrocycles. However, K_a of **1a**·6ClO_4 and **1b**·6ClO_4 with naphthalene were higher than those of tetracationic cyclophane, $ExBox^{4+}$ and naphthalene, 0.286 ± 0.011 ×10^3 dm^3 mol^{-1}. The 6+ charge of the $\mathbf{1}^{6+}$ macrocycle, as well as the size and shape compatibility between naphthalene and **1a**·6ClO_4 and **1b**·6ClO_4 may be responsible for this observation[24]. On contrary, $ExBox^{4+}$ demonstrated K_a values of 0.883 ± 0.140 ×10^3 dm^3 mol^{-1} and 1.38 ± 0.016 ×10^3 dm^3 mol^{-1} for anthracene and phenanthrene that were higher than those of anthracene and phenanthrene observed in this work for complexation with **1a**·6ClO_4 and **1b**·6ClO_4. The three-dimensional hexa-cationic $ExCage^{6+}$ demonstrated K_a values of 2.82 ± 0.70 ×10^3 dm^3 mol^{-1} 62.2 ± 2.6 ×10^3 dm^3 mol^{-1} for complexation with naphthalene and phenanthrene[26] which were greater than those observed in this work for the complexation of naphthalene and phenanthrene with **1a**·6ClO_4 and **1b**·6ClO_4. Although the $ExCage^{6+}$ and $\mathbf{1}^{6+}$ have the same charge, the size and the shape of the three-dimensional cavity and the 1,3,5-tris(4-pyridyl)-benzene and *p*-xylylene units in the $ExCage^{6+}$ are responsible for the strong π–π stacking between the electron-deficient 'host' and the electron-rich 'guest' leading an increase in the value of K_a by one to two orders of magnitude[26].

Quenching constant

In the presence of a cationic quencher, $\mathbf{1}^{6+}$, the fluorescence-active naphthalene, anthracene and phenanthrene demonstrate fluorescence quenching which evidences the complexation between $\mathbf{1}^{6+}$ and PAHs. Linearity of the Stern-Volmer plots of $\mathbf{1}^{6+}$ and PAHs (Figure 4d for $\mathbf{1b}^{6+}$-phenanthrene complex as an example) indicates that the fluorescence quenching of PAHs by $\mathbf{1a}^{6+}$ takes place via a dynamic quenching mechanism.

The Stern-Volmer plots of the various $\mathbf{1}^{6+}$-PAH combinations result in the K_{sv} values for these combinations (Table 1). Among the two macrocycles studied, $\mathbf{1a}^{6+}$ demonstrates lower K_{sv} values with linear acenes, naphthalene and anthracene, than does $\mathbf{1b}^{6+}$. On the contrary, K_{sv} for the quenching of phenanthrene by $\mathbf{1a}^{6+}$ (153.99 ± 0.67 dm^3 mol^{-1}) is higher than that of $\mathbf{1b}^{6+}$ (134.57 ±1.30 dm^3 mol^{-1}).

Moreover, K_a and K_{sv} of $\mathbf{1a}^{6+}$ and $\mathbf{1b}^{6+}$ with linear acenes, naphthalene and anthracene, exhibit an inversely proportional relationship. In contrast, K_a and K_{sv} of $\mathbf{1a}^{6+}$ and $\mathbf{1b}^{6+}$ with phenanthrene demonstrate a directly proportional relationship.

Table 1. Stoichiometries, binding constants K_a and Stern-Volmer quenching constants K_{sv} of $\mathbf{1}^{6+}$ and PAH complexes.

Polycyclic aromatic hydrocarbon	Stoichiometry		Binding constant (K_a) dm^3 mol^{-1}		Stern-Volmer quenching constant (K_{SV}) dm^3 mol^{-1}	
	$\mathbf{1a}^{6+}$	$\mathbf{1b}^{6+}$	$\mathbf{1a}^{6+}$	$\mathbf{1b}^{6+}$	$\mathbf{1a}^{6+}$	$\mathbf{1b}^{6+}$
Naphthalene	1:1	1:1	476.60 ± 0.84	420.66 ± 0.63	69.17 ± 0.97	72.21 ± 1.73
Anthracene	1:1	1:1	410.42 ± 0.75	340.91 ± 0.66	110.43 ± 1.47	116.87 ± 1.10
Phenanthrene	1:1	1:1	495.84 ± 2.65	459.61 ± 1.96	153.99 ± 0.67	134.57 ± 1.30

Conclusion

In this work, the complexation between two protonated hexaazacyclophane macrocycles, $\mathbf{1a}^{6+}$ and $\mathbf{1b}^{6+}$, and PAHs, naphthalene, anthracene, and phenanthrene, was investigated. DFT calculations confirm that the dimensions and electronic properties of $\mathbf{1}^{6+}$ make them electronically compatible to undergo complexation with PAHs. Solution phase studies of each combination of $\mathbf{1}^{6+}$ with PAH demonstrate 1:1 stoichiometric complexation between $\mathbf{1}^{6+}$ and PAH. The $\mathbf{1}^{6+}$-phenanthrene complexes thereby showed the highest values for the binding constant K_a and for the quenching constant K_{SV}. On the other hand, the $\mathbf{1}^{6+}$-anthracene complexes showed the lowest value of K_a, while the $\mathbf{1}^{6+}$-naphthalene complexes showed the lowest value of K_{SV}. The cavity geometry of $\mathbf{1}^{6+}$ and the shape and number of fused benzenoid rings of PAH contribute to the binding constant between $\mathbf{1}^{6+}$ and PAH. In order to confirm the encapsulation

of PAHs in $\mathbf{1}^{6+}$, solid-state single crystal X-ray diffraction analysis of each complex of $\mathbf{1}^{6+}$ and PAHs needs to be carried out. The findings of this reporting study can be adopted to develop $\mathbf{1}^{6+}$ and PAHs complexation-driven removal of PAHs from PAH-contaminated water.

Acknowledgement

The authors are grateful to the Research Council, University of Sri Jayewardenepura, Sri Lanka, for funding this research project with the University Research Grant, grant number ASP/01/RE/SCI/2017/09. The authors would like to further extend their acknowledgement to the Department of Chemistry and the Instrument Center at the Faculty of Applied Sciences, University of Sri Jayewardenepura, Sri Lanka, and the Sri Lanka Institute of Nanotechnology, Sri Lanka, for providing access to the necessary physical resources and the instrumentation facilities used in this research project.

References

[1] Hayakawa, K., *Polycyclic Aromatic Hydrocarbons*, Springer, Gateway East, Singapore, **2018**.

[2] Patel, A. B.; Shaikh, S.; Jain, K. R.; Desai, C.; Madamwar, D., *Front. Microbiol.*, **2020**, *11*, 562813 (23 pages).

[3] Lawal, A. T., *Cogent Environ. Sci.*, **2017**, *3*, 1339841 (89 pages).

[4] Reizer, E.; Viskolcz, B.; Fiser B., *Chemosphere*, **2022**, *291*, 132793 (15 pages).

[5] Mallah, M. A.; Changxing, L.; Mallah, M. A.; Noreen, S.; Liu, Y.; Saeed, M.; Xi, H.; Ahmed, B.; Feng, F.; Mirjat, A. A.; Wang, W.; Jabar, A.; Naveed, M.; Li, J.-H.; Zhang, Q., *Chemosphere*, **2022**, *296*, 133948 (24 pages).

[6] Honda, M.; Suzuki, N., *Int. J. Environ. Res. Public Health* **2020**, *17*, 1363 (23 pages).

[7] Sun, K.; Song, Y.; He, F.; Jing, M.; Tang, J.; Liu, R., *Sci. Total Environ.*, **2021**, *773*, 145403 (19 pages).

[8] Paris, A.; Ledauphin, J.; Poinot, P.; Gaillard, J. L., *Environ. Pollut.*, **2018**, *234*, 96–106.

[9] Thacharodi, A.; Hassan, S.; Singh, T.; Mandal, R.; Jeganathan, Khan, H. A.; Hussain, M. A.; Pugazhendhi, A., *Chemosphere*, **2023**, *328*, 138498 (18 pages).

[10] Ghosal, D.; Ghosh, S.; Dutta, T. K.; Ahn, Y., *Front. Microbiol.*, **2016**, *7*, 1369 (27 pages).

[11] Smol, M.; Włodarczyk-Makuła, M., *Polycycl. Aromat. Compd.*, **2017**, *37*, 292–313.

[12] Singh, P.; Ojha, A.; Borthakur, A.; Singh, R.; Lahiry, D.; Tiwary, D.; Mishra, P. K.; *Environ. Sci. Pollut. Res.*, **2016**, *23*, 22340–22364.

[13] Nguyen, V. H.; Phan Thi, L. A.; Van Le, Q.; Singh, P.; Raizada, P.; Kajitvichyanukul, P., *Chemosphere* **2020**, *260*, 127529 (16 pages).

[14] Wang, Q.; Liu, M.; Li, Y.; Liu, Y.; Li, S.; Ge, R., *Atmos. Environ.*, **2016**, *144*, 175–181.

[15] Mojiri, A.; Zhou, J. L.; Ohashi, A.; Ozaki, N.; Kindaichi, T., *Sci. Total Environ.*, **2019**, *696*, 133971 (16 pages).

[16] Kumar, M.; Bolan, N. S.; Hoang, S. A.; Sawarkar, A. D.; Jasemizad, T.; Gao, B.; Keerthanan, S.; Padhye, L. P.; Singh, L.; Kumar, S.; Vithanage, M.; Zhang, Y.; Li, M.; Kirkham, M. B.; Vinu, A. Rinklebe, J., *J. Hazard. Mater.*, **2021**, *420*, 126534 (25 pages).

[17] Fenyvesi, É.; Sohajda, T., *Environ. Sci. Pollut. Res.*, **2022**, *29*, 20085–20097.

[18] Branco, T. J. F.; Vieira Ferreira, L. F.; Botelho do Rego, A. M.; Oliveira, A. S.; Da Silva, J. P., *Photochem. Photobiol. Sci.*, **2006**, *5*, 1068–1077.

[19] Morillo, E.; Madrid, F.; Lara-Moreno, A.; Villaverde, J., *Int. J. Pharm.*, **2020**, *591*, 119943 (24 pages).

[20] Kim, H. J.; Lee, M. H.; Mutihac, L.; Vicens, J.; Kim, J. S., *Chem. Soc. Rev.*, **2012**, *41*, 1173–1190.

[21] García, M. D.; Alvariño, C.; López-Vidal, E. M.; Rama, T.; Peinador, C.; Quintela, J. M., *Inorganica Chim. Acta* **2014**, *417*, 27–37.

[22] Tamgho, I. S.; Chaudhuri, S.; Verderame, M.; DiScenza, D. J.; Levine, M., *RSC Adv.*, **2017**, *7*, 28489–28493.

[23] Spenst, P.; Sieblist, A.; Würthner, F., *Chem. - A Eur. J.*, **2017**, *23*, 1667–1675.

[24] Barnes, J. C.; Juríček, M.; Strutt, N. L.; Frasconi, M.; Sampath, S.; Giesener, M. A.; McGrier, P. L.; Bruns, C. J.; Stern, C. L.; Sarjeant, A. A.; Stoddart, J. F., *J. Am. Chem. Soc.*, **2013**, *135*, 183–192.

[25] Juríček, M.; Barnes, J. C.; Dale, E. J.; Liu, W. G.; Strutt, N. L.; Bruns, C. J.; Vermeulen, N. A.; Ghooray, K. C.; Sarjeant, A. A.; Stern, C. L.; Botros, Y. Y.; Goddard, W. A.; Stoddart, J. F., *J. Am. Chem. Soc.*, **2013**, *135*, 12736–12746.

[26] Dale, E. J.; Vermeulen, N. A.; Thomas, A. A.; Barnes, J. C.; Juricek, M.; Anthea, K.; Strutt, N. L.; Sarjeant, A. A.; Stern, C. L.; Denmark, S. E.; Stoddart, J. F., *J. Am. Chem. Soc.*, **2014**, *136*, 10669–10682.

[27] Habibi, D.; Izadkhah, V., *Phosphorus, Sulfur Silicon Relat. Elem.*, **2004**, *179*, 1197–1202.

[28] Clifford, T.; Danby, A. M.; Lightfoot, P.; Richens, D. T.; Hay, R. W., *J. Chem. Soc. Dalt. Trans.*, **2001**, *30*, 240–246.

[29] Menif, R.; Martell, A. E.; Squattrito, P. J.; Clearfield, A.; *Inorg. Chem.*, **1990**, *29*, 4723–4729.

[30] Menif, R., *J. Chem. Soc., Chem. Commun.*, **1989**, *25*, 1521–1523.

[31] Zagwinski, J.; Lehn, J.-M.; Méric, R.; Vigneron, J.-P.; Cesario, J. M.; Guilhem, J.; Pascard, C., *Tetrahedron Lett.*, **1987**, *28*, 3489–3492.

[32] Jobs, P., *Ann. Chim.*, **1928**, *9*, 113–203.

[33] Thordarson, P., *Chem. Soc. Rev.*, **2011**, *40*, 1305–1323.

[34] Benesi, H. A.; Hildebrand, J. H., *J. Am. Chem. Soc.*, **1949**, *71*, 2703–2707.

[35] Wahba, M. E. K.; El-Enany,N.; Belal, F., *Anal. Methods*, **2015**, *7*, 10445–10451.

[36] Gehlen, M. H.; *J. Photochem. Photobiol. C Photochem. Rev.*, **2020**, *42*, 100338 (39 pages).

[37] Poater, J.; Duran, M.; Solà, M., *Front. Chem.*, **2018**, *6*, 561 (14 pages).

[38] Dale, E. J.; Vermeulen, N. A.; Juríček, M.; Barnes, J. C.; Young, R. M.; Wasielewski, M. R.; Stoddart, J. F., *Acc. Chem. Res.*, **2016**, *49*, 262–273.